PHYSICAL REVIEW B **94**, 121113(R) (2016)

Observation of Fermi arcs in the type-II Weyl semimetal candidate WTe_2

Yun Wu,[1,2] Daixiang Mou,[1,2] Na Hyun Jo,[1,2] Kewei Sun,[1] Lunan Huang,[1,2] S. L. Bud'ko,[1,2] P. C. Canfield,[1,2,*] and Adam Kaminski[1,2,†]

[1]*Ames Laboratory, U.S. DOE, Iowa State University, Ames, Iowa 50011, USA*

[2]*Department of Physics and Astronomy, Iowa State University, Ames, Iowa 50011, USA*

(Received 21 April 2016; revised manuscript received 22 June 2016; published 14 September 2016)

We use ultrahigh resolution, tunable, vacuum ultraviolet laser angle-resolved photoemission spectroscopy (ARPES) to study the electronic properties of WTe_2, a material that was predicted to be a type-II Weyl semimetal. The Weyl fermion states in WTe_2 were proposed to emerge at the crossing points of electron and hole pockets, and Fermi arcs connecting electron and hole pockets would be visible in the spectral function on (001) surface. Here we report the observation of such Fermi arcs in WTe_2 confirming the theoretical predictions. This provides strong evidence for type-II Weyl semimetallic states in WTe_2. We also find that trivial and topological domains coexist on the same surface of the sample due to the presence of inhomogeneous strain detected by scanning electron microscopy data. This is in agreement with the theoretical prediction that strain can drive this system from topological Weyl to trivial semimetal. WTe_2 therefore provides a tunable playground for studying exotic topological quantum effects.

DOI: 10.1103/PhysRevB.94.121113

The discovery of graphene [1] opened the possibility to study relativistic quasiparticles that can be realized in solids. The occurrence of Dirac dispersion attracted great interest and triggered searches for novel topological states in three-dimensional (3D) systems [2,3]. Dirac semimetals with bulk 3D Dirac points protected by crystal symmetry have been proposed to exist in β-cristobalite BiO_2 [4] and A_3Bi (A = Na, K, Rb) [5] and experimentally confirmed in Na_3Bi and Cd_3As_2 [6–12]. This led to the observation of novel topological quantum states with Fermi arcs [13,14], which were first observed in Na_3Bi [15]. Subsequently, another type of massless particle—the Weyl fermion [16]—was predicted to exist in a family of noncentrosymmetric transition-metal monophosphides [17,18]. Angle-resolved photoemission spectroscopy (ARPES) measurements on TaAs [19–22] and NbAs [23] confirmed the existence of Fermi arcs connecting Weyl points of opposite chirality. Recently, a new type of Weyl semimetal (type-II Weyl semimetal) was proposed to possess Weyl points emerging at the boundary between electron and hole pockets [24]. WTe_2 [24] and $MoTe_2$ [25] were among the first predicted to be type-II Weyl semimetals with different Fermi arc lengths. By doping Mo in WTe_2, the Fermi arc length (or the topological strength) can be continuously tuned [26]. Signatures of topological Fermi arcs have been reported in Mo-doped WTe_2 by using pump laser techniques to access the states above the Fermi level [27]. Spectroscopic evidence for type-II Weyl semimetal states in $MoTe_2$ was reported and novel "track states" were predicted by theoretical modeling and density functional theory calculations [28] and subsequently discovered by ARPES [29]. In addition to W(Mo)Te_2 family [27,29–33], $YbMnBi_2$ [34], and LaAlGe [35] were also reported to display signatures of type-II Weyl semimetal states.

WTe_2 has attracted great interest due to its extremely large magnetoresistance at low temperatures and high magnetic fields [36], which resemble those of the earlier studied $PtSn_4$ [37,38]. Superconductivity has been reported to emerge from a suppressed magnetoresistive state by applying high pressure [39,40]. Interestingly, a temperature induced Lifshitz transition has also been observed in WTe_2 caused by dramatic shifts of the chemical potential with temperature [41]. Type-II Weyl semimetal states have also been proposed to exist in WTe_2 [24]. However, the Weyl points reside roughly 50 meV above the Fermi level and are separated by just a few meV, making it difficult to be observed by ARPES measurements. Fortunately, the Weyl points project to distinct locations on the (001) surface and Fermi arcs should emerge connecting electron and hole pockets with opposite Chern number [24]. This distinct topological surface state can be easily observed by ARPES measurements. Although the band structures and Fermi surface of WTe_2 have been reported previously [41–43], no surface states were clearly observed.

Here, we present the study of the electronic structure of WTe_2 by using an ultrahigh resolution, tunable, vacuum ultraviolet (vuv) laser-based ARPES system. We observed two pairs of Fermi arcs that link the electron and hole pockets. These features are consistent with the theoretical prediction that this material is a host of the type-II Weyl semimetallic state. Our results, together with reports of similar states in $MoTe_2$ [27,29], point to the (W,Mo)Te_2 systems as exciting platforms for tuning the properties of Weyl fermions [26]. WTe_2, in particular, is a model system, where the topological properties can be turned on and off and tuned by the use of strain.

Whereas most of the previous measurements have been carried out on WTe_2 crystals grown via chemical vapor transport using halogens as transport agents [36,44], we have grown WTe_2 single crystals from a Te-rich binary melt. High purity, elemental W and Te were placed in alumina crucibles in W_1Te_{99} and W_2Te_{98} ratios. The crucibles were sealed in amorphous silica tubes and the ampoules were heated to 1000 °C over 5 h, held at 1000 °C for 10 h, and then slowly cooled to 460 °C over 100 h and finally decanted using a centrifuge [45]. The resulting crystals were blade-

*canfield@ameslab.gov
†kaminski@ameslab.gov

or ribbonlike in morphology with typical dimensions of $3 \times 0.5 \times 0.01$ mm.

Samples for ARPES measurements were cut to roughly a square shape (approximatetly 300×300 μm) and cleaved *in situ* at 16 and 40 K under ultrahigh vacuum (UHV). The data were acquired using a tunable vuv laser ARPES system, consisting of a Scienta R8000 electron analyzer, picosecond Ti:sapphire oscillator, and fourth harmonic generator [46]. Data were collected with tunable photon energies from 5.3 to 6.7 eV. Momentum and energy resolution were set at $\sim$0.005 Å^{-1} and 1 meV, respectively. The size of the photon beam on the sample was set at $\sim$30 μm.

The schematic drawing of the crystal structure of single unit cell layer of WTe_2 is shown in Fig. 1(a). This structure breaks the inversion symmetry due to slight differences in the bond lengths between tungsten and tellurium within the unit cell. This results in the tellurium layer on each side of tungsten being inequivalent. We label whose as "A" and "B." We indeed observed two distinct types of electronic structures, but even for a single cleave there were often two different domain types present. This is illustrated in panels (b)–(e) where we show the picture of the sample after cleaving and data along cut #4 (marked in panel h, between the hole and electron pockets) for three spots are plotted in panels (c)–(e). The data from the part of the sample marked by a red circle in (b) shows sharp electronlike dipersion near the E_F. The data near the edge of the sample [green and blue circles in (b)] partially (d) or completely (e) lacks this feature. The two domains have different Fermi surfaces and band dispersions as demonstrated in Fig. 1. The Fermi surface of type N (normal) domain is shown in panel (f) and the band dispersion along the Γ-X symmetry direction is plotted in panel (g). These data are very similar to what was previously reported [41]. Figure 1(h) shows the Fermi surface plot for the type T (topological) domains in the first Brillouin zone, integrated within 10 meV about the chemical potential, with the high intensity contours marking the location of the Fermi surface crossings. The presence of Fermi arcs that connect the bulk hole and electron pockets is clearly visible. This is further confirmed by examining the band dispersions along cuts #1–#6 as shown in Figs. 1(i) and 1(j)–1(n). In addition to the two nearly degenerate electron bands and two branches on the left side of the hole pockets (marked by the red dashed lines), a high intensity, sharp band dispersion can be clearly seen, that connects the bottom of the electron pockets and the top of the hole pockets. The data along the y-axis cuts shown in Figs. 1(j)–1(n), for the type T domains look almost the same as the type N domains [41], except for cuts #3 and #4. Here, an additional electron band is present that results in the formation of the Fermi arcs seen in Fig. 1(h). We will examine this feature in more detail below. The data from more than a dozen samples had both features present on cleaved surfaces. We also cleaved and measured the same piece of single crystal on both sides. We found the presence of both domains on each side. The presence of two types of domain on the same side of the sample is inconsistent with the scenario of two different surface terminations, as for a given piece of sample, cleaving it on one side should consistently yield either type "A" or "B," but not both [see Fig. 1(a)]. Residual strain introduced by cutting and/or cleaving of the samples is responsible for the

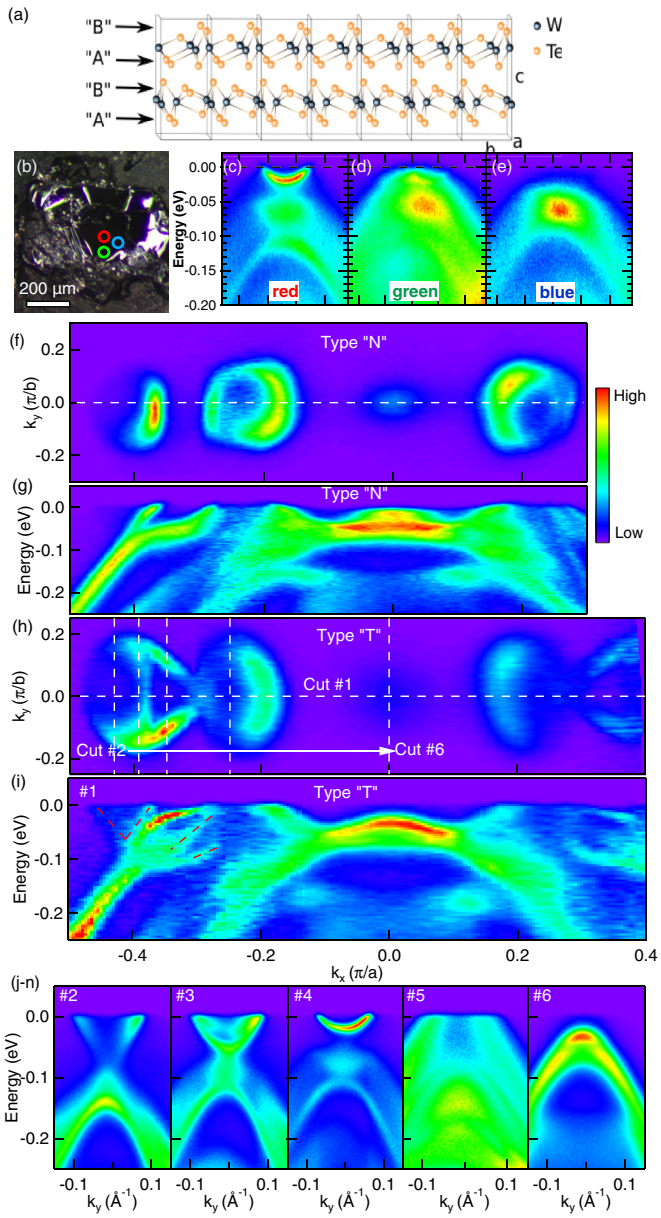

FIG. 1. Two types of Fermi surface plot and band dispersion measured at photon energy of 6.7 eV. (a) Schematic drawing of the crystal structure of single unit cell layer with two possible cleaving sites marked by arrows. Note that these are not equivalent to "N" and "T" data types. (b) Optical image of the cleaved sample with three measured regions marked by circles. (c)–(e) Data measured in red, green, and blue regions marked in (b), respectively. (f) Type "N" Fermi surface plot of ARPES intensity integrated within 10 meV about the chemical potential measured at $T = 40$ K. (g) Band dispersion along white dashed line cut in (f). (h) Type "T" Fermi surface plot of ARPES intensity integrated within 10 meV about the chemical potential measured at $T = 16$ K. (l)–(n) Band dispersions along cuts #1–#6 in (h). Red dashed lines in (i) mark the electron pocket and two left branches of the hole bands.

two different electronic structures. This is consistent with the theoretical prediction that the topological character of WTe_2 is highly sensitive to pressure and strain [24]. In particular, it was theoretically demonstrated that stretching the crystal

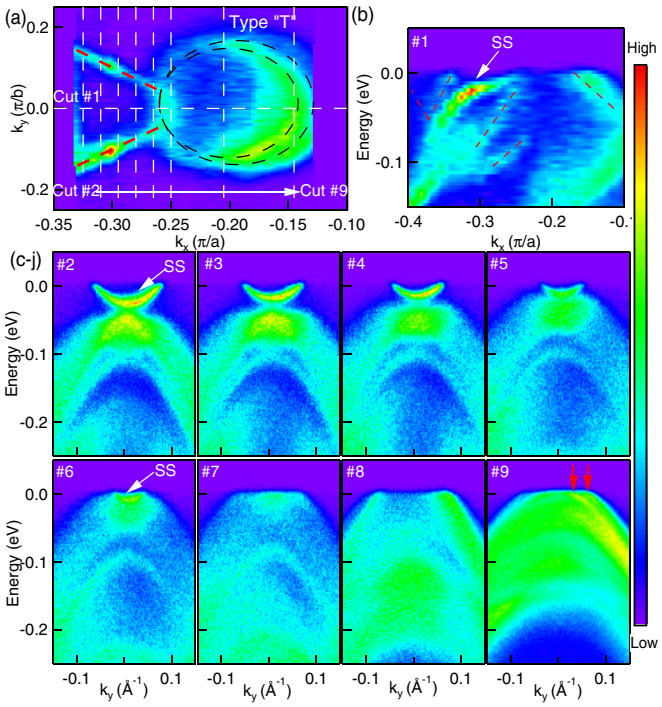

FIG. 2. Fermi surface plot and band dispersion measured at T = 16 K and photon energy of 6.7 eV. (a) Fermi surface plot of ARPES intensity integrated within 5 meV about the chemical potential. The red dashed line marks the contour of the surface state (SS) and the black dashed lines mark the contour of the two bulk hole pockets. (b)–(j) Band dispersion along cuts #1–#9. Dashed lines in (b) mark the electron pocket and the two hole pockets. The white arrows point to the location of the SS. The red arrows in (j) point to the locations of the two hole bands crossing Fermi level.

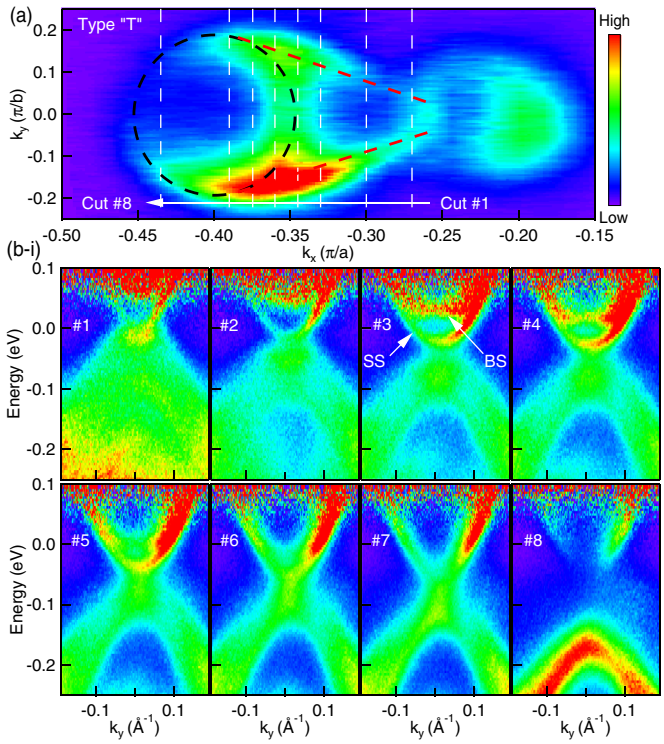

FIG. 3. Fermi surface plot and band dispersion measured at T = 160 K and photon energy of 6.7 eV. (a) Fermi surface plot of ARPES intensity integrated within 10 meV about the chemical potential. The red dashed line marks the contour of the SS and the black dashed line marks the contour of the bulk electron pocket. (b)–(i) Band dispersion along cuts #1–#8. The white arrows point to the location of the SS and the bulk state (BS).

along the a and c axis causes annihilation of the Weyl points and transition from topological to trivial semimetal. In type N (normal) domains the Fermi surface consists of two pairs of electron pockets and two pairs of hole pockets in agreement with previous studies [41–43] and bulk band calculations, where the Fermi arcs are absent.

Figure 2 shows details of the Fermi sheets and band dispersion of what we will show is an unusual surface state. In panel (a) we plot the ARPES intensity (integrated within 5 meV about the chemical potential) close to the momentum region, where the surface state connects to the hole pocket. The red dashed line and the black dashed lines in Fig. 2(a) mark the outline of the surface electron pockets and two almost degenerate hole pockets, respectively. The band dispersion along cut #1 is shown in Fig. 2(b), where the white arrow points to the location of the surface state. Detailed band dispersions along the white vertical cuts are shown in Figs. 2(c)–2(j). The bottom of this surface band dips only slightly below the E_F demonstrating its electron character. This band is much sharper than the lower energy broad, bulk hole bands, consistent with its surface origin. As we move towards the zone center, the electron band shrinks and moves closer to the Fermi level, while the lower hole bands move up. The Fermi arc surface state touches the hole bands at cut #5 [panel (f)] and is completely swallowed by the lower hole bands along cut #6 [panel (g)]. After cut #6, the hole bands continue moving up and finally cross the Fermi level and form a pair of hole pockets. We can clearly see the separation of the almost degenerate hole pockets along cut #9 [panel (j)], as marked by the red arrows pointing at the crossing points.

The merging between Fermi arcs and bulk electron pockets is shown in Fig. 3. Panel (a) shows the ARPES intensity integrated within 10 meV about the chemical potential and measured at T = 160 K. The black dashed line and red dashed line mark the location of the bulk electron pockets and Fermi arc band, respectively. In order to better show the details of the bulk electron pockets, we have plotted the ARPES intensity divided by the Fermi function along the white vertical cuts #1–#8 in Figs. 3(b)–3(i). At cut #1 [panel (b)], a single electron pocket is clearly observed that touches the top of the lower hole bands and forms the beginning of two Fermi arcs on either side. As we move away from the hole pockets, the band responsible for Fermi arcs moves to higher binding energy. Slightly further (cut #2) a bulk band becomes visible still above the E_F. Both bands are very clearly visible starting from cut #3, where they are indicated by white arrows and labeled. Closer to the center of the bulk electron pocket, the two bands eventually merge together. The detailed band evolution in Figs. 2 and 3 demonstrates that the Fermi arc states connect the bottom of the electron pockets and the top of the hole pockets, consistent with the previous theoretical prediction [24].

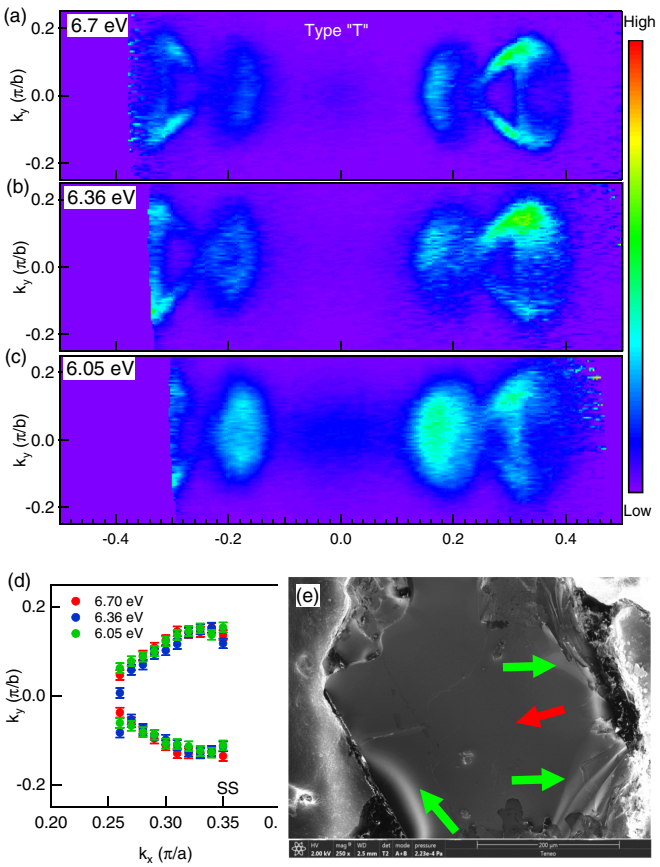

FIG. 4. Fermi surface plot measured at $T = 40$ K. (a)–(c) Fermi surface plot of ARPES intensity integrated within 10 meV about the chemical potential measured at photon energies of 6.7, 6.36, and 6.05 eV, respectively. (d) Fermi surface contour extracted from peak positions of momentum dispersion curves. (e) Scanning electron microscopy (SEM) image of cleaved sample surface. The red arrow points to the flat area close to the sample center, while green arrows point to areas away from the center where buckling and thus strain is present.

To verify the surface origin of the Fermi arc band, we have carried out photon energy dependent measurements and present them in Fig. 4. Panels (a)–(c) show the ARPES intensity integrated within 10 meV about the chemical potential measured at photon energies of 6.7, 6.36, and 6.05 eV, respectively. We can clearly see that the shape of the bulk electron pockets and hole pockets change slightly with photon energy, but the Fermi arcs that connect them remain sharp and its central part does not. To better quantify our results, we have plotted the contour obtained by fitting to the data of the Fermi arc band in Fig. 4(d). The outlines of the central section of the Fermi arcs remains the same for all three photon energies. As discussed previously [24,26,29], the electronic structure of WTe_2 and $MoTe_2$ may change significantly even if a small change in the lattice parameters (e.g., strain) is considered in band structure calculations. By performing high precision SEM measurements using various backscattering geometries we found that close to the center of the sample, the surface is relatively flat. Closer to the edges of the cleaved sample, where ARPES data shows mostly N-type domains, we observed buckling of the sample surface which demonstrates the presence of strain as shown in Fig. 4(e).

In summary, we have used ultrahigh resolution, tunable, laser-based ARPES to study the electronic properties of WTe_2, a compound that was predicted to be a type-II Weyl semimetal. We found two different cleave types that have distinct electronic structure. The first type is consistent with previous studies, while the second type displays clear Fermi arcs that connect the hole and electron pockets. The coexistence of the trivial and topological domains is most likely due to the presence of inhomogeneous strain, which can tune topological properties of this material [24]. The Fermi arcs reported here are long sought after signatures of the type-II Weyl semimetallic state that were predicted by theory [24].

Note added. Recently, we become aware of results presenting ARPES data that are consistent with ours [47–49]. We note that Bruno *et al.* [47] considers the observed surface state topologically trivial and inconclusive to establish the presence of a type-II Weyl state. While it is true that Weyl points in WTe_2 are too high above the E_F to be observed directly with ARPES, given the rarity of Fermi arcs in solid state and good agreement between data and theory prediction we argue that our interpretation is a very reasonable one. We are not aware of any other theory that could explain the presence of Fermi arcs in a trivial material.

We would like to thank Nandini Trivedi and Tim McCormick for very useful discussions and Matthew Kramer for assistance with SEM experiments. Research was supported by the U.S. Department of Energy, Office of Basic Energy Sciences, Division of Materials Sciences and Engineering. Ames Laboratory is operated for the U.S. Department of Energy by the Iowa State University under Contract No. DE-AC02-07CH11358. N.H.J. is supported by the Gordon and Betty Moore Foundation EPiQS Initiative (Grant No. GBMF4411). L.H. was supported by CEM, a NSF MRSEC, under Grant No. DMR-1420451.

Y.W. and D.M. contributed equally to this work.

[1] A. K. Geim and K. S. Novoselov, Nat. Mater. **6**, 183 (2007).
[2] M. Z. Hasan and C. L. Kane, Rev. Mod. Phys. **82**, 3045 (2010).
[3] X.-L. Qi and S.-C. Zhang, Rev. Mod. Phys. **83**, 1057 (2011).
[4] S. M. Young, S. Zaheer, J. C. Y. Teo, C. L. Kane, E. J. Mele, and A. M. Rappe, Phys. Rev. Lett. **108**, 140405 (2012).
[5] Z. Wang, Y. Sun, X.-Q. Chen, C. Franchini, G. Xu, H. Weng, X. Dai, and Z. Fang, Phys. Rev. B **85**, 195320 (2012).
[6] Z. Wang, H. Weng, Q. Wu, X. Dai, and Z. Fang, Phys. Rev. B **88**, 125427 (2013).
[7] Z. K. Liu, B. Zhou, Y. Zhang, Z. J. Wang, H. M. Weng, D. Prabhakaran, S.-K. Mo, Z. X. Shen, Z. Fang, X. Dai, Z. Hussain, and Y. L. Chen, Science **343**, 864 (2014).

[8] M. Neupane, S.-Y. Xu, R. Sankar, N. Alidoust, G. Bian, C. Liu, I. Belopolski, T.-R. Chang, H.-T. Jeng, H. Lin, A. Bansil, F. Chou, and M. Z. Hasan, Nat. Commun. **5**, 3786 (2014).

[9] Z. K. Liu, J. Jiang, B. Zhou, Z. J. Wang, Y. Zhang, H. M. Weng, D. Prabhakaran, S.-K. Mo, H. Peng, P. Dudin, T. Kim, M. Hoesch, Z. Fang, X. Dai, Z. X. Shen, D. L. Feng, Z. Hussain, and Y. L. Chen, Nat. Mater. **13**, 677 (2014).

[10] H. Yi, Z. Wang, C. Chen, Y. Shi, Y. Feng, A. Liang, Z. Xie, S. He, J. He *et al.*, Sci. Rep. **4**, 6106 (2014).

[11] S. Borisenko, Q. Gibson, D. Evtushinsky, V. Zabolotnyy, B. Büchner, and R. J. Cava, Phys. Rev. Lett. **113**, 027603 (2014).

[12] A. Narayanan, M. D. Watson, S. F. Blake, N. Bruyant, L. Drigo, Y. L. Chen, D. Prabhakaran, B. Yan, C. Felser, T. Kong, P. C. Canfield, and A. I. Coldea, Phys. Rev. Lett. **114**, 117201 (2015).

[13] X. Wan, A. M. Turner, A. Vishwanath, and S. Y. Savrasov, Phys. Rev. B **83**, 205101 (2011).

[14] G. Xu, H. Weng, Z. Wang, X. Dai, and Z. Fang, Phys. Rev. Lett. **107**, 186806 (2011).

[15] S.-Y. Xu, C. Liu, S. K. Kushwaha, R. Sankar, J. W. Krizan, I. Belopolski, M. Neupane, G. Bian, N. Alidoust, T.-R. Chang, H.-T. Jeng, C.-Y. Huang, W.-F. Tsai, H. Lin, P. P. Shibayev, F.-C. Chou, R. J. Cava, and M. Z. Hasan, Science **347**, 294 (2015).

[16] H. Weyl, Z. Phys. **56**, 330 (1929).

[17] S.-M. Huang, S.-Y. Xu, I. Belopolski, C.-C. Lee, G. Chang, B. Wang, N. Alidoust, G. Bian, M. Neupane, C. Zhang, S. Jia, A. Bansil, H. Lin, and M. Z. Hasan, Nat. Commun. **6**, 7373 (2015).

[18] H. Weng, C. Fang, Z. Fang, B. A. Bernevig, and X. Dai, Phys. Rev. X **5**, 011029 (2015).

[19] S.-Y. Xu, I. Belopolski, N. Alidoust, M. Neupane, G. Bian, C. Zhang, R. Sankar, G. Chang, Z. Yuan, C.-C. Lee *et al.*, Science **349**, 613 (2015).

[20] L. X. Yang, Z. K. Liu, Y. Sun, H. Peng, H. F. Yang, T. Zhang, B. Zhou, Y. Zhang, Y. F. Guo, M. Rahn, D. Prabhakaran, Z. Hussain, S. Mo, C. Felser, B. Yan, and Y. L. Chen, Nat. Phys. **11**, 728 (2015).

[21] B. Q. Lv, N. Xu, H. M. Weng, J. Z. Ma, P. Richard, X. C. Huang, L. X. Zhao, G. F. Chen, C. E. Matt, F. Bisti, V. N. Strocov, J. Mesot, Z. Fang, X. Dai, T. Qian, M. Shi, and H. Ding, Nat. Phys. **11**, 724 (2015).

[22] B. Q. Lv, H. M. Weng, B. B. Fu, X. P. Wang, H. Miao, J. Ma, P. Richard, X. C. Huang, L. X. Zhao, G. F. Chen, Z. Fang, X. Dai, T. Qian, and H. Ding, Phys. Rev. X **5**, 031013 (2015).

[23] S. Xu, N. Alidoust, I. Belopolski, Z. Yuan, G. Bian, T. Chang, H. Zheng, V. N. Strocov, D. S. Sanchez, G. Chang *et al.*, Nat. Phys. **11**, 748 (2015).

[24] A. A. Soluyanov, D. Gresch, Z. Wang, Q. Wu, M. Troyer, X. Dai, and B. A. Bernevig, Nature (London) **527**, 495 (2015).

[25] Y. Sun, S.-C. Wu, M. N. Ali, C. Felser, and B. Yan, Phys. Rev. B **92**, 161107 (2015).

[26] T.-R. Chang, S.-Y. Xu, G. Chang, C.-C. Lee, S.-M. Huang, B. Wang, G. Bian, H. Zheng, D. S. Sanchez, I. Belopolski *et al.*, Nat. Commun. **7**, 10639 (2016).

[27] I. Belopolski, S.-Y. Xu, Y. Ishida, X. Pan, P. Yu, D. S. Sanchez, M. Neupane, N. Alidoust, G. Chang, T.-R. Chang *et al.*, Phys. Rev. B **94**, 085127 (2016).

[28] T. M. McCormick, I. Kimchi, and N. Trivedi, arXiv:1604.03096.

[29] L. Huang, T. M. McCormick, M. Ochi, Z. Zhao, M.-t. Suzuki, R. Arita, Y. Wu, D. Mou, H. Cao, J. Yan *et al.*, Nature Materials (2016).

[30] K. Deng, G. Wan, P. Deng, K. Zhang, S. Ding, E. Wang, M. Yan, H. Huang, H. Zhang, Z. Xu *et al.*, arXiv:1603.08508 [Nature Phys. (to be published)].

[31] J. Jiang, Z. Liu, Y. Sun, H. Yang, R. Rajamathi, Y. Qi, L. Yang, C. Chen, H. Peng, C.-C. Hwang *et al.*, arXiv:1604.00139.

[32] A. Liang, J. Huang, S. Nie, Y. Ding, Q. Gao, C. Hu, S. He, Y. Zhang, C. Wang, B. Shen *et al.*, arXiv:1604.01706.

[33] N. Xu, Z. Wang, A. Weber, A. Magrez, P. Bugnon, H. Berger, C. Matt, J. Ma, B. Fu, B. Lv *et al.*, arXiv:1604.02116.

[34] S. Borisenko, D. Evtushinsky, Q. Gibson, A. Yaresko, T. Kim, M. N. Ali, B. Buechner, M. Hoesch, and R. J. Cava, arXiv:1507.04847v2.

[35] S.-Y. Xu, N. Alidoust, G. Chang, H. Lu, B. Singh, I. Belopolski, D. Sanchez, X. Zhang, G. Bian, H. Zheng *et al.*, arXiv:1603.07318.

[36] M. N. Ali, J. Xiong, S. Flynn, J. Tao, Q. D. Gibson, L. M. Schoop, T. Liang, N. Haldolaarachchige, M. Hirschberger, N. P. Ong, and R. J. Cava, Nature (London) **514**, 205 (2014).

[37] E. Mun, H. Ko, G. J. Miller, G. D. Samolyuk, S. L. Bud'ko, and P. C. Canfield, Phys. Rev. B **85**, 035135 (2012).

[38] Y. Wu, L.-L. Wang, E. Mun, D. D. Johnson, D. Mou, L. Huang, Y. Lee, S. L. Bud'ko, P. C. Canfield, and A. Kaminski, Nat. Phys. **12**, 667 (2016).

[39] D. Kang, Y. Zhou, W. Yi, C. Yang, J. Guo, Y. Shi, S. Zhang, Z. Wang, C. Zhang, S. Jiang, A. Li, K. Yang, Q. Wu, G. Zhang, L. Sun, and Z. Zhao, Nat. Commun. **6**, 7804 (2015).

[40] X.-C. Pan, X. Chen, H. Liu, Y. Feng, Z. Wei, Y. Zhou, Z. Chi, L. Pi, F. Yen, F. Song, X. Wan, Z. Yang, B. Wang, G. Wang, and Y. Zhang, Nat. Commun. **6**, 7805 (2015).

[41] Y. Wu, N. H. Jo, M. Ochi, L. Huang, D. Mou, S. L. Bud'ko, P. C. Canfield, N. Trivedi, R. Arita, and A. Kaminski, Phys. Rev. Lett. **115**, 166602 (2015).

[42] I. Pletikosic, M. N. Ali, A. V. Fedorov, R. J. Cava, and T. Valla, Phys. Rev. Lett. **113**, 216601 (2014).

[43] J. Jiang, F. Tang, X. C. Pan, H. M. Liu, X. H. Niu, Y. X. Wang, D. F. Xu, H. F. Yang, B. P. Xie, F. Q. Song, P. Dudin, T. K. Kim, M. Hoesch, P. K. Das, I. Vobornik, X. G. Wan, and D. L. Feng, Phys. Rev. Lett. **115**, 166601 (2015).

[44] B. E. Brown, Acta Crystallogr. **20**, 268 (1966).

[45] P. C. Canfield and Z. Fisk, Philos. Mag. B **65**, 1117 (1992).

[46] R. Jiang, D. Mou, Y. Wu, L. Huang, C. D. McMillen, J. Kolis, H. G. Giesber, J. J. Egan, and A. Kaminski, Rev. Sci. Instrum. **85**, 033902 (2014).

[47] F. Y. Bruno, A. Tamai, Q. S. Wu, I. Cucchi, C. Barreteau, A. de la Torre, S. M. Walker, S. Riccò, Z. Wang, T. K. Kim, M. Hoesch, M. Shi, N. C. Plumb, E. Giannini, A. A. Soluyanov, and F. Baumberger, Phys. Rev. B **94**, 121112 (2016).

[48] C. Wang, Y. Zhang, J. Huang, S. Nie, G. Liu, A. Liang, Y. Zhang, B. Shen, J. Liu, C. Hu *et al.*, arXiv:1604.04218 .

[49] B. Feng, Y.-H. Chan, Y. Feng, R.-Y. Liu, M.-Y. Chou, K. Kuroda, K. Yaji, A. Harasawa, P. Moras, A. Barinov, W. G. Malaeb, C. Bareille, T. Kondo, S. Shin, F. Komori, T.-C. Chiang, Y. Shi, and I. Matsuda, arXiv:1606.00085 .